Astron. Astrophys. 326, 897–906 (1997)

ASTRONOMY AND ASTROPHYSICS

Near-infrared surface photometry of spiral galaxies⋆

II. Derivation of mass models

Ph. Héraudeau and F. Simien

CRAL-Observatoire de Lyon, F-69561 Saint-Genis-Laval Cedex, France

Received 3 June 1996 / Accepted 9 May 1997

Abstract. Near-infrared surface photometry of six spiral galaxies is used to separate the main stellar components and derive mass models whose predicted rotation curves are compared to observed gas kinematics. For three of the galaxies, central stellar velocity dispersions are also used. For these intrinsically bright objects, the mass-to-light ratio of the disk, in the K band, is found to be $\simeq 1$, as expected. In four Sb-Sc galaxies, there is some evidence that the mass-to-light ratio of the bulge may be on average $\simeq 20$ % smaller, but the a priori assumption that these ratios are identical does not significantly bias the disk masses. Early-type spirals with a prominent bulge, in which the apparent central mass-to-light ratio is known to be often low, can need a significant correction to the bulge mass.

Key words: galaxies: spiral – galaxies: photometry – galaxies: kinematics and dynamics – infrared: galaxies – galaxies: structure

1. Introduction

Most studies on the global distribution of mass within the optical extent of spiral galaxies have relied on one (or both) of the following sets of data: the gas kinematics and the surface photometry. Several early works used to derive a mass density directly from the observed rotation curve (e.g., Burbidge et al. 1959; Brandt 1960); more recent studies have often used the surface-brightness distribution to derive a model rotation curve which, fitted to the observed one, determines one or more mass-to-light ($\mathscr{M}/L$) ratios, depending on the number of components adding up their contributions (e.g., Wielen 1976; Monnet & Simien 1977; Kent 1986, 1987, 1988; Broiels & Courteau 1997).

Send offprint requests to: F. Simien (simien@obs.univ-lyon1.fr)

⋆ Based in part on observations collected at the European Southern Observatory, La Silla, Chile, and at the Observatoire de Haute-Provence, France.

In this paper, adopting the second method, we aim at determining the large-scale distribution of mass in a few galaxies, selected for the availability of: a) near-infrared (NIR) surface photometry, so that the observed luminosity is not strongly affected by extinction, especially in the central regions, b) I-band surface photometry for the extrapolation of the NIR data, and, c) gas or stellar kinematics.

A basic requirement for a straightforward interpretation of the derived $\mathscr{M}/L$ ratios is that the stellar light be a good tracer of the overall mass distribution in the range of the rotation-curve fitting. Since it is widely accepted that the fraction of dark matter within the optical region is anticorrelated to the total luminosity (Persic & Salucci 1988; Persic et al. 1996, hereafter PSS96), we have limited our analysis to intrinsically bright galaxies.

The paper is organized as follows: Sect. 2 presents all the data; in Sect. 3, we calculate the space density of luminosity, starting from a separation of the main stellar components; then, the kinematical information is used to determine the $\mathscr{M}/L$ ratios: the gas rotation (in Sect. 4) and, for three galaxies, the bulge velocity dispersion (Sect. 5). The results are discussed in Sect. 6, and Sect. 7 presents a short conclusion.

2. The data

2.1. Sample characteristics

From the 30-object sample of NIR observations in Héraudeau et al. (1996a; hereafter HSMa), we have selected six galaxies with large angular dimensions ($D_{25} > 2'$) and favorable inclination ($i \simeq 70°$); they also span a wide range of bulge-to-disk ratios. A few relevant parameters are presented in Table 1. All these objects are unbarred (even NGC 7541: see HSMa); one of them is a Seyfert 2 (NGC 6810).

These six objects have high intrinsic luminosities, $-21.8 \leq M_B \leq -20.7$; they are characterized by $M_I \lesssim -22.1$: for spirals in this range, at a radius $r \simeq 0.7\frac{D_{25}}{2}$ corresponding, typically, to the beginning of the rotation plateau, the average contribution of the dark matter is less than $\simeq 16$ % in square velocity (PSS96: their Fig. 6).

Table 1. Catalog elements for program galaxies

Object	Type	B_T	I_T	K_T	Δ	M_B	D_{25}	ϵ
(1)	(2)	(3)	(4)	(5)	(6)	(7)	(8)	(9)
ESO 320-26	Sb	12.79	10.92	8.71	36	−21.1	144	0.63
NGC 6788	Sab	12.81	10.62	8.53	40	−21.4	174	0.66
NGC 6810	Sab	12.29	10.05	7.81	23	−20.7	180	0.73
NGC 7083	Sc	11.88	10.36	8.23	38	−21.8	216	0.45
NGC 7541	Sbc	12.41	10.75	8.44	36	−21.8	198	0.73
NGC 7606	Sb	11.56	9.78	8.01	30	−21.5	288	0.56

Notes. Col. (2): Type, morphological type (from the *LEDA* database - status: LEDA1996); col. (3): B_T, integrated blue magnitude (*LEDA*); col. (4): I_T, integrated I-band magnitude (from Héraudeau & Simien 1996 for NGC 7541; from Mathewson et al. 1992 – MFB92 – for the other galaxies); col. (5): K_T, integrated K-band magnitude (HSMa); col. (6): Δ, distance in Mpc, from radial velocity corrected for Virgocentric infall, with H_0 = 75 km s^{-1} Mpc^{-1} (*LEDA*); col. (7): M_B, absolute blue magnitude, from B_T corrected for Galactic extinction and for inclination (*LEDA*); col. (8): D_{25}, apparent diameter at brightness level μ_B = 25, in arcsec (*LEDA*); col. (9): ϵ, ellipticity of the disk outer isophotes (HSMa).

2.2. Surface photometry

The K'-band frames of HSMa were obtained at the ESO/MPI 2.20-m telescope at La Silla. As usual with K' data, their outward extent is reduced, mainly because of the brightness and fluctuations of the sky level, and an extrapolation is needed. For this, the I band is likely the best choice, since it allows much deeper observations, and since the hypothesis of a constant $I-K'$ color in the outer regions is not too questionable; so, for five out of six galaxies, we have made use of the I profiles of Mathewson et al. (1992: hereafter MFB92), and for NGC 7541 we have used an I frame obtained at the Observatoire de Haute-Provence (Héraudeau & Simien 1996).

The merging of the K'- and I-band data was made as follows; for each galaxy, we defined: a) an isophote setting the outer boundary of the reliable K' data, b) a slightly larger isophote setting the inner boundary of the adopted I data, and, c) the shift in brightness applied to the I profile to avoid a discontinuity; we then generated the combined image, with a smooth transition between K' and I in the domain delimited by the two above-mentioned ellipses. This transition zone was, typically, situated at radius $r \simeq 60''$ and surface brightness $\mu_{K'} \simeq 19$.

With these extrapolations, brightness values are available well beyond the range of the rotation curves, a necessary requirement, as we will see below (Sect. 4.1).

2.3. Gas rotation

We have used optical measurements of emission lines along the major axis. For NGC 7541, the data are from Rubin et al. (1980). For the other galaxies, we have used the rotation curves of MFB92; these two studies give high-quality measurements, with an accuracy of $\simeq 20$ km s^{-1} on individual points.

For NGC 6788, the inner part of the rotation curve is significantly asymmetric with respect to the central position indicated by MFB92; so, we adopted for the center an offset of $2.3''$ (Persic & Salucci 1995), which resulted in a better balanced fitting by the model (Sect. 4.1).

2.4. Stellar velocity dispersion

The central velocity dispersion of the bulge, determined from absorption spectroscopy, is available for three objects:

- NGC 7083: $\sigma_0 = 74 \pm 16$ km s^{-1} (Whitmore & Rubin 1985: hereafter WR85)
- NGC 7541: $\sigma_0 = 67 \pm 36$ km s^{-1} (WR85)
- NGC 7606: two determinations have been made. The first one is by Whitmore & Malamuth (1984): $\sigma_0 = 160 \pm 20$ km s^{-1}. The second one comes from observations at the 1.93-m telescope of the Observatoire de Haute-Provence, equipped with the *CARELEC* long-slit spectrograph (Héraudeau & Simien, in preparation); the selected setup provided a spectral resolution of 104 km s^{-1} per pixel, and a spatial resolution of $1.2''$ per pixel along the slit. With a Fourier-Fitting method, we found a central dispersion of $\sigma_0 = 137 \pm 20$ km s^{-1}, a value which we will adopt in the present paper.

All these dispersions were determined with a gaussian fitting to the line-of-sight velocity distribution (LOSVD).

3. Space density of luminosity

For the calculation of the 3D density, we have considered the following stellar components:

- a moderately flattened, oblate bulge, whose iso-density surfaces are similar ellipsoids; its luminosity obeys the $r^{1/n}$ law in projection (Sérsic 1968), which is a generalization of the $r^{1/4}$ law of de Vaucouleurs, and which has recently been shown to be suited to small- and intermediate-size bulges (Andredakis et al. 1995).
- a highly flattened, axisymmetric disk (termed 'old' disk), with an exponential fall-off (Freeman 1970). The intrinsic geometry is that of a thin sheet with an exponential decrease of density away from the equatorial plane, and with a constant scale height; we adopt a ratio of the effective dimensions (perpendicular/parallel to the plane) of z_e/r_e = 0.05. This crude model lacks the physical significance of the isothermal sheet used by, e.g., van der Kruit & Searle (1981), but it is adapted to the present work. The isophotes are also assumed to be well approximated by similar ellipses.
- a spiral-arm component superposed to the axisymmetric disk.

Our model is then characterized by the following elements: a) for the bulge, the semi-major axis r_e and the surface brightness μ_e of the effective isophote containing half the total light of this component, its ellipticity ϵ, and the exponent n of the density law, b) for the disk, a set of corresponding r_e, μ_e and ϵ parameters; and, c) for the arms, the map of the surface intensity in excess of the bulge+disk model.

We have fitted the above model to our six galaxies. Starting with an eyeball estimate of the bulge and disk components, we first determined the best disk parameters in a region covering the NIR data and part of the I extension (in a range variable from one object to another). This was done by minimizing the sum of the square residuals between the bulge+disk model and the 2D data, assigning a different weight to positive and negative residuals in order to bring out the arm contribution. Then, the PSF-convolved bulge model was optimized in the central region. When necessary, a further iteration was performed.

Application of this method led to the following comments:

- in the disk of several galaxies, there is significant uncertainty on the relative brightnesses of the old-disk and spiral-arm components; however, since we have found no evidence for a different $\mathscr{M}/L$ ratio, this uncertainty can be considered as a second-order effect; then, the main purpose of the arm separation, as performed here, is twofold: a) to allow a better estimate of the old-disk axial ratio, and hence of the inclination angle, and, b) to bring out the features of the flat component entering the inner region of the bulge; these features are usually incipient spiral arms, or dust patterns which can still be present at K' (the morphology of our galaxies is detailed in HSMa and in Héraudeau et al. 1996c);
- the central, bulge-dominated region is smooth but the inner features, when present, distort the isophotes significantly (NGC 6810 is a revealing example). In this case, a fine tuning based on a 'guided fitting' had to follow the process described above; then, a careful visual inspection of the map of the residuals allowed us to check that we had properly accounted for the bulge structure.

For the reasons above, characterizing the quality of the fit by a global χ^2 or a similar parameter would not be very significant. However, when a direct fit to the bulge was possible, then the rms residual within this range was usually better than 0.1 mag.

The results of the component separation are presented as photometric profiles in Figs. 1 to 6, and the derived parameters are listed in Table 2 (starting with this Table, all photometric quantities have been converted from the K' band to the K band for easier subsequent comparisons to other works).

At this stage, the 3D density of luminosity in the galaxy is fully determined by the additional knowledge of: a) the inclination i of the galaxy with respect to the plane of the sky, as derived from the disk flattening, and b) the assumption that the arm component has the same (small) thickness as the axisymmetric disk.

Table 2. Results of the photometric analysis

	Bulge					Disk		
Object	r_e	μ_e	ϵ	n	$L/L_{\rm T}$	r_e	μ_e	ϵ
(1)	(2)	(3)	(4)	(5)	(6)	(7)	(8)	(9)
ESO 320-26	2.4	15.10	0.41	1.7	0.13	35.4	18.39	0.63
NGC 6788	15.5	18.15	0.40	4.0	0.39	39.0	18.53	0.75
NGC 6810	10.1	16.44	0.40	6.0	0.47	35.0	17.98	0.78
NGC 7083	7.5	17.79	0.20	3.3	0.19	35.8	18.69	0.54
NGC 7541	4.3	16.65	0.37	2.1	0.11	38.5	18.07	0.69
NGC 7606	4.8	16.64	0.37	1.8	0.08	56.3	18.66	0.56

Notes. Col. (2): r_e, semi-major axis of the bulge effective isophote, containing half the total luminosity of this component, in arcsec; col. (3): μ_e, surface brightness along the effective isophote, converted to K mag arcsec^{-2} (we have adopted $K - K' = -0.06$); col. (4): apparent ellipticity of the bulge (1− apparent axial ratio); col. (5): n, exponent of the $r^{1/n}$ luminosity law (Sérsic 1968); col. (6): $L/L_{\rm T}$, bulge-to-total luminosity ratio, in the K band; cols. (7)-(9): same as cols. (2)-(4), for the disk.

4. Circular rotation

4.1. Rotation of the models

For the bulge model, we have used the classic formulae of Burbidge et al. (1959) to calculate the circular rotation velocity.

The rotation of the disk deserves two particular comments:

- Several works have adopted a geometry with similar, and highly flattened, ellipsoidal iso-density surfaces (e.g., Burbidge et al. 1959; Monnet & Simien 1977); in this case, a point in the equatorial plane is insensitive to the potential of the outer ellipsoids. It is well known that this is not true for an infinitely thin disk (Lequeux 1983 ; Binney & Tremaine 1987), nor for a sheet of constant thickness; thus, an extrapolation is needed beyond the outermost point where the rotation is to be determined.
- We have found that the rotation is not critically dependent on the assumed scale-height: doubling $z_{\rm e}$, for instance, only changes the square velocity by a few percents.

For the non-axisymmetric arm component, we have merely added up the contributions of all pixels, taking into account the spread of mass perpendicularly to the plane; a similar method (but with zero thickness) had previously been used by Kalnajs (1983), Buchhorn & Mathewson (1992), Simien & Héraudeau (1994), Héraudeau et al. (1996b; hereafter HSMb). This relies on the hypothesis that the overall potential is axisymmetric enough, so that its radial derivative provides a sufficient approximation to the motion of the gas, even near the spiral arms.

The model rotation curve, obtained by combining the contributions of the three components (after assigning respective $\mathscr{M}/L$ ratios) was projected onto the plane of the sky for a direct comparison to the observations.

4.2. Reliability of the gas

Our results will show that, to a first approximation, the radial motions in the vicinity of the spiral arms can be neglected, for the present objects.

In the central regions, it is well-known that the motion of the gas does not always trace the circular rotation: it is often slower, it can also be faster. On the one hand, several phenomena can lead to small apparent rotations, like non-planar geometry, ring-like geometry in the case of edge-on galaxies, or large turbulent motions (see, e.g., Fillmore et al. 1986; Kent 1988; Bertola et al. 1995; Kormendy et al. 1996 and references therein). On the other hand, several authors have reported high observed rotation of

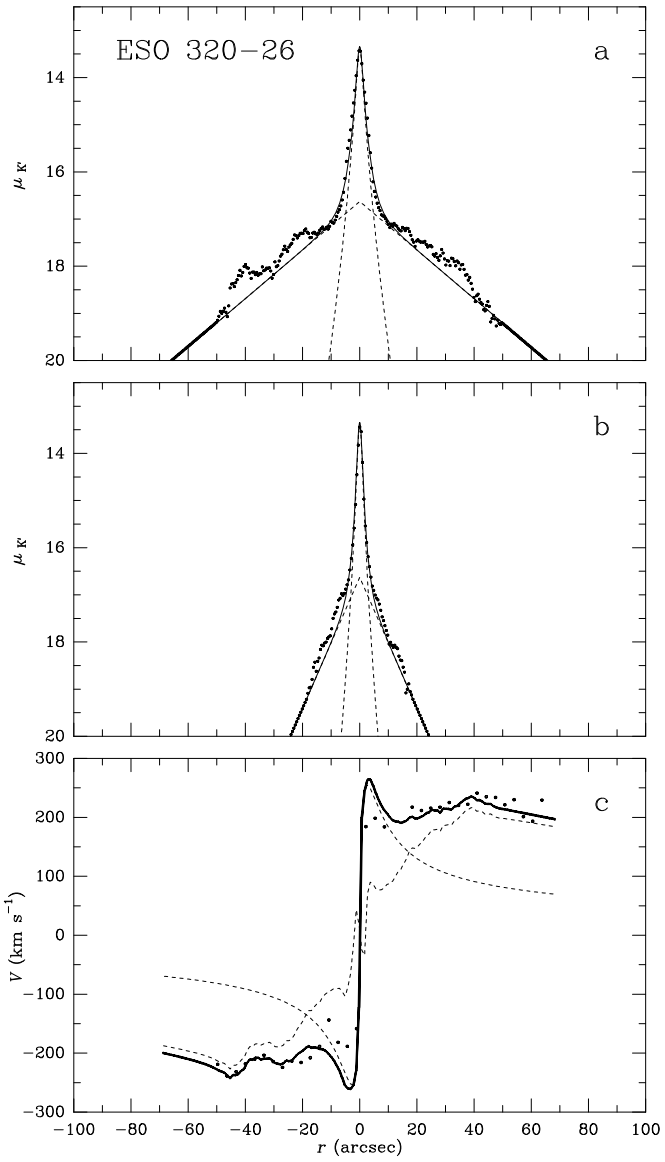

Fig. 1a–c. Photometric and kinematical fits for ESO 320-26. **a** major-axis profiles; *dots*: K'-band data extrapolated by I-band data; *dashed lines*: PSF-convolved bulge with $r^{1/n}$ projected law, and exponential axisymmetric disk; *solid line*: bulge+disk model. **b** minor-axis profiles. **c** circular rotation curves; *dots*: gas observations from MFB92; *dashed lines*: calculated bulge and disk+arms contributions, with the same $\mathscr{M}/L$ ratio; *solid line*: resultant model rotation

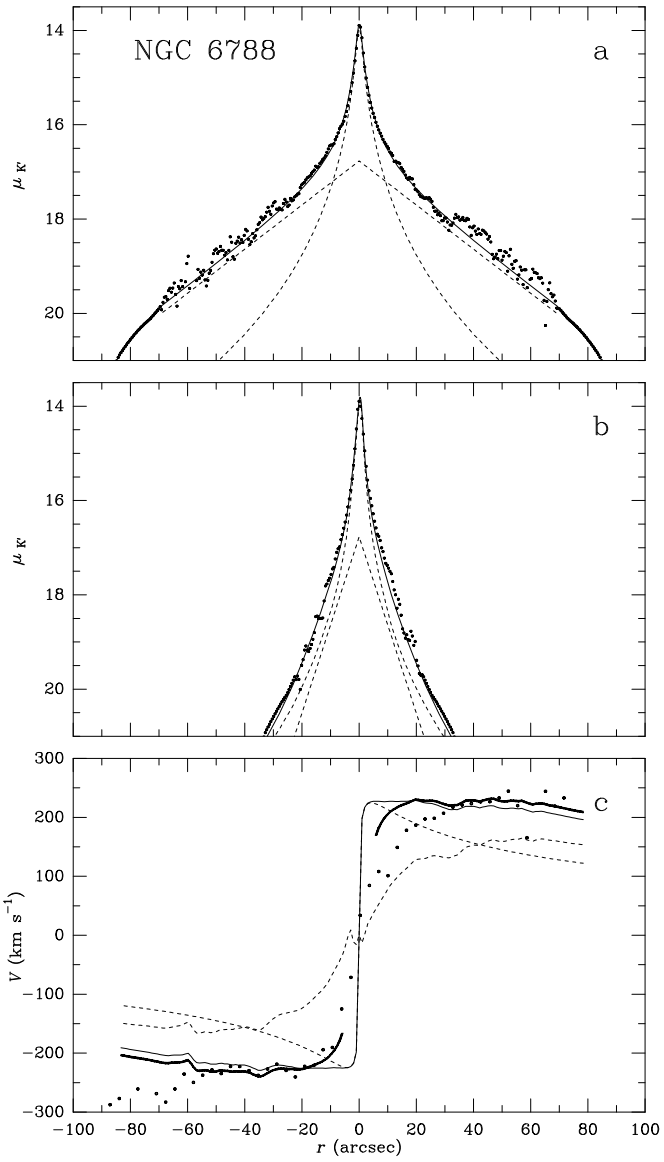

Fig. 2a–c. Same as Fig. 1, for NGC 6788. **c** *thin solid line*: resultant model rotation for $\mathscr{M}/L$ = 1.1; *thick solid line*: model rotation for $\mathscr{M}/L$ = 1.3 and a correction to the central mass of the bulge (see Sect. 4.3)

the gas near the center (e.g., Rubin & Graham 1987; Afanasiev et al. 1989; Sofue 1996, to cite only a few), and they often argue for the presence of a compact central mass; except for the cases where the problem can actually be settled by a careful analysis of the light distribution (e.g., Simien & Héraudeau 1994), many galaxies may indeed exhibit a rotation more rapid than predicted by the bulge.

Whatever the type and the sense of the discrepancy, a better estimate of the bulge $\mathscr{M}/L$ is obtained if we exclude the innermost region from the rotation-curve fitting. So, we made the conservative choice of limiting the fitting to $r > r_{\rm e}$, i.e., outside the bulge effective radius, with a minimum distance of $5''$ from the center.

4.3. Fits to the rotation curves

We have determined $\mathscr{M}/L$ ratios by minimizing the sum of the square residuals between the observed rotation curve and the model, in the above-defined range. For an easier comparison to other results, we have collected in Appendix A and Table 4 several determinations from the literature; the expected value is $\mathscr{M}/L \simeq 1$ in the K band, for both the bulge and the disk.

Table 3. $\mathscr{M}/L$ determinations from rotation-curve fitting

	Solution 1			
Object	Bulge	Disk	Solution 2	Solution 3
(1)	(2)	(3)	(4)	(5)
ESO 320-26	0.77	1.30	1.20	
NGC 6788	0.58	1.70	1.10	1.30
NGC 6810	0.28	1.10	0.53	0.70
NGC 7083	0.48	1.00	0.84	
NGC 7541	0.72	0.96	0.90	
NGC 7606	1.40	1.70	1.60	

Notes. Listed values correspond to the K band. 'Solution 1' is an unconstrained fit with two free parameters, the bulge and disk $\mathscr{M}/L$ ratios, whose derived values are given in cols. (2) and (3); 'solution 2' is a fit with the condition $(\mathscr{M}/L)_{\rm B} = (\mathscr{M}/L)_{\rm D}$ ($f = 1$); 'solution 3' imposes the same condition, but with a correction lowering the mass of the innermost region of the bulge (see Sect. 4.3).

Our data did not show a different value for the old disk and the arms, and subsequently we will consider only two (possibly different) ratios, $(\mathscr{M}/L)_{\rm B}$ for the bulge and $(\mathscr{M}/L)_{\rm D}$ for the flat component (the disk, for short); for the sake of simplicity, let us define $f = (\mathscr{M}/L)_{\rm B}/(\mathscr{M}/L)_{\rm D}$. We have performed three different kinds of fitting, which are detailed below, and whose results are summarized in Table 3.

1) We first tried two free parameters, $(\mathscr{M}/L)_{\rm B}$ and $(\mathscr{M}/L)_{\rm D}$; in all cases, we found $f < 1$ and, for the two galaxies with a very large bulge contribution (NGC 6788 and NGC 6810 [1]), this ratio ($f \simeq 0.6$ and 0.3 respectively) is particularly low compared to the expected $f \simeq 1$. $(\mathscr{M}/L)_{\rm D}$ has an average value of 1.3 with a rms scatter of 0.3.

2) Next, we considered only one free parameter, with the condition $f = 1$; for NGC 6810 the solution is unrealistic: at $r = 50''$, i.e., deep into the disk ($r \simeq 0.6\frac{D_{25}}{2}$) the bulge still dominates the contributions to the rotation velocity, and $(\mathscr{M}/L) = 0.53$ is anomalously low for the disk, compared to all other galaxies. For the five remaining galaxies, $(\mathscr{M}/L)_{\rm D}$ has an average value of 1.1 with a rms scatter of 0.3. For NGC 6788, we note a large discrepancy between the model and gas rotations at $r \lesssim 20''$. For the four remaining galaxies, the adopted rotation curves are shown as a thick solid line in Figs. 1, 4, 5, and 6.

3) NGC 6810 obviously needs another solution, and deserves a closer look. As already mentioned, it is classified Seyfert 2. Appendix B recalls several effects which can contribute to increasing the central luminosity of the bulge. Although it is beyond the scope of the present study to quantify these effects in the case of NGC 6810, we adopt there existence as a working hypothesis; a hint that this may indeed be the case comes from the high Sérsic exponent, $n = 6$, of the bulge luminosity law, which mimics a very condensed central spike; but due to the limited resolution, this evidence is only marginal. We calculated that a central mass correction lowering by $0.8 \times 10^{10} \mathscr{M}_\odot$ the bulge mass within $r \simeq 5''$, with $f = 1$ and $\mathscr{M}/L$=0.7, produces a reasonable fit to the observed rotation curve; this correction corresponds to $\simeq 23\%$ of the whole bulge mass. Although NGC 6788 has no reported AGN, we have applied the same technique to reduce the discrepancy of the rotation at $r \lesssim r_{\rm e}$: we found a mass correction of $10^{10} \mathscr{M}_\odot$, representing $\simeq 17\%$ of its bulge mass.

These $\mathscr{M}/L$ ratios will be discussed in Sect. 6.

[1] The bulge mass-to-light ratio given by HSMb was unfortunately in error.

5. Dynamical model

For a few objects, we have used stellar dynamics with the aim of tightening the constraints on the bulge $\mathscr{M}/L$. As a starting point, we have considered a two-component structure (bulge and axisymmetric disk), to represent the innermost region; for such a system, supposed in a stationary state, and with only two isolating integrals of motion, the Jeans' equations write, in cylindrical coordinates (r, θ, z):

$$\frac{\partial}{\partial z}(\nu\sigma_r^2) = -\nu\frac{\partial\Phi}{\partial z}, \qquad (1a)$$

$$\frac{\partial}{\partial r}(\nu\sigma_r^2) - \frac{\nu}{r}(\Theta_{\rm m}^2 + \sigma_\theta^2 - \sigma_r^2) = \nu\frac{\partial\Phi}{\partial r}, \qquad (1b)$$

where the σ_r, σ_θ and σ_z components of the velocity dispersion refer to either stellar population; $\Theta_{\rm m}$ is the mean rotation velocity, and ν the space density of luminosity of this same population; Φ is the total gravitational potential, incorporating the $\Phi_{\rm B}$ and $\Phi_{\rm D}$ contributions (bulge and disk, respectively).

Using the ν distributions calculated in Sect. 3, and the $\mathscr{M}/L$ values from Sect. 4.1, we solved Eqs. (1) for the bulge in the isotropic case ($\sigma_r = \sigma_z = \sigma_\theta$). After some experimentation, we reached the following conclusions:

- the outer part of the bulge is incompatible with the assumption of isotropy, if the geometry is conserved (this would lead to negative values of $\Theta_{\rm m}^2$): it is clear that the response of the bulge to the highly flattened $\Phi_{\rm D}$ should be taken into account.
- the velocity-dispersion profile of the bulge is also sensitive to the scale-height $z_{\rm e}$ of the disk.

This provided ample evidence that an elaborate, two-component model was beyond the scope of the present study, and we restricted ourselves to the bulge, as if it were self gravitating; given the compactness of this component in the three galaxies considered (NGC 7083, NGC 7541, and NGC 7606), this was not too crude. After solving the simplified Eqs. (1), we projected the dispersions and the mean velocities onto the plane of the sky, we averaged within a (typical) slit of width $2.2''$; next, we analyzed the resulting LOSVD with a gaussian fitting in the Fourier domain, in order to simulate the reduction of actual galaxy spectra, and we adjusted the $(\mathscr{M}/L)_{\rm B}$ ratio to match the calculated velocity dispersion to the observed σ_0. This led to the following results:

- for NGC 7083, $(\mathscr{M}/L)_{\rm B} = 0.4 \pm 0.2$, a low value consistent with the unconstrained fit to the gas rotation.

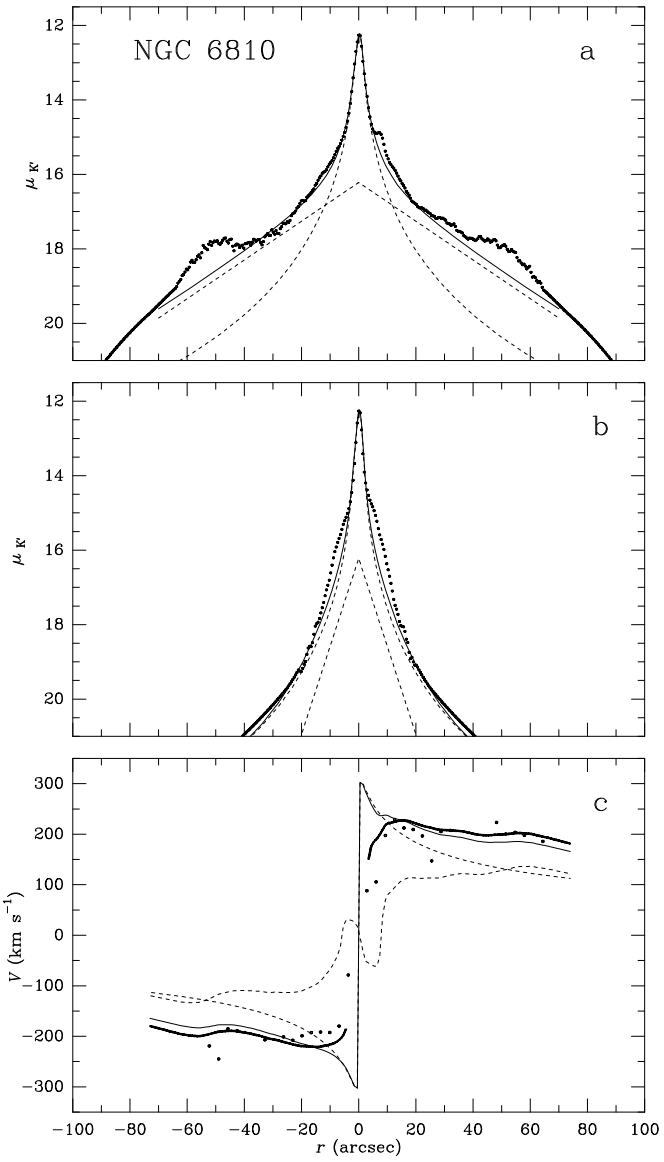

Fig. 3a–c. Same as Fig. 1, for NGC 6810. **c** *thin solid line*: resultant model rotation for $\mathscr{M}/L$ = 0.53; *thick solid line*: model rotation for $\mathscr{M}/L$ = 0.70 and a correction to the central mass of the bulge (see Sect. 4.3)

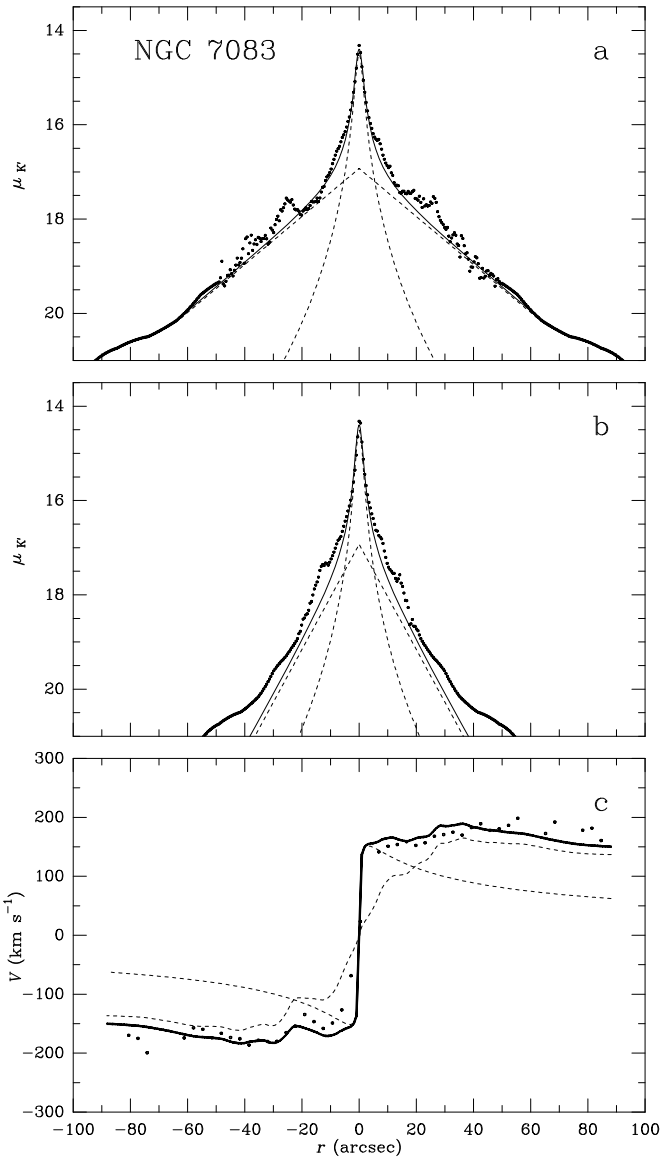

Fig. 4a–c. Same as Fig. 1, for NGC 7083

- for NGC 7541, $(\mathscr{M}/L)_B = 0.5^{+1.2}_{-0.4}$; the large error bar due the low accuracy on the measured σ_0 brackets the two different determinations shown in Table 3.
- for NGC 7606, we found a troublesome value of $(\mathscr{M}/L)_B = 2.3 \pm 0.5$. Unless both determinations of σ_0 are aberrant, the discrepancy could be due to: a) an inadequate hypothesis of self gravity for the bulge: indeed, a Φ_D would bring the result down to $(\mathscr{M}/L)_B \simeq 1.8$, a value still surprisingly high; or, b) a prolate or triaxial geometry and an anisotropic dynamics increasing the dispersion and lowering the mean rotation. We also note that all $\mathscr{M}/L$ determinations for the bulge and disk of this galaxy are significantly greater than 1, this may possibly be related to a distance error.

6. Discussion

6.1. The overall distribution of luminosity and mass

The separation of bulge, disk, and arm components leads to a satisfactory determination of the light distribution in the main stellar components. Our data are not constraining enough to enter the recent debate on whether the K' light does trace accurately the stellar masses (Rix & Rieke 1993; Rix & Zaritsky 1995), or does not (Gnedin et al. 1995; Rhoads 1996), a question which is presently restricted to large and highly resolved galaxies like M 51 and M100; we have thus based our analysis on the assumption that the former statement holds. Except for the central region of two out of six galaxies, our model rotation curves fit the observed ones reasonably well, with most of the

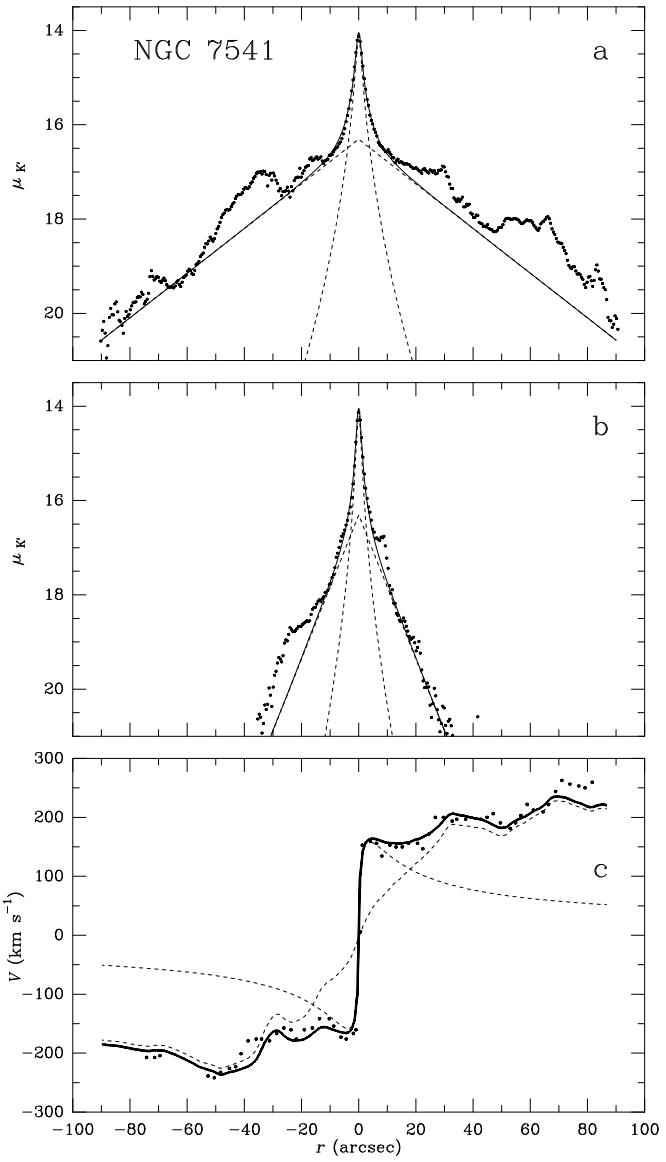

Fig. 5a–c. Same as Fig. 1, for NGC 7541. For this galaxy, the gas rotation curve is from Rubin et al. (1980)

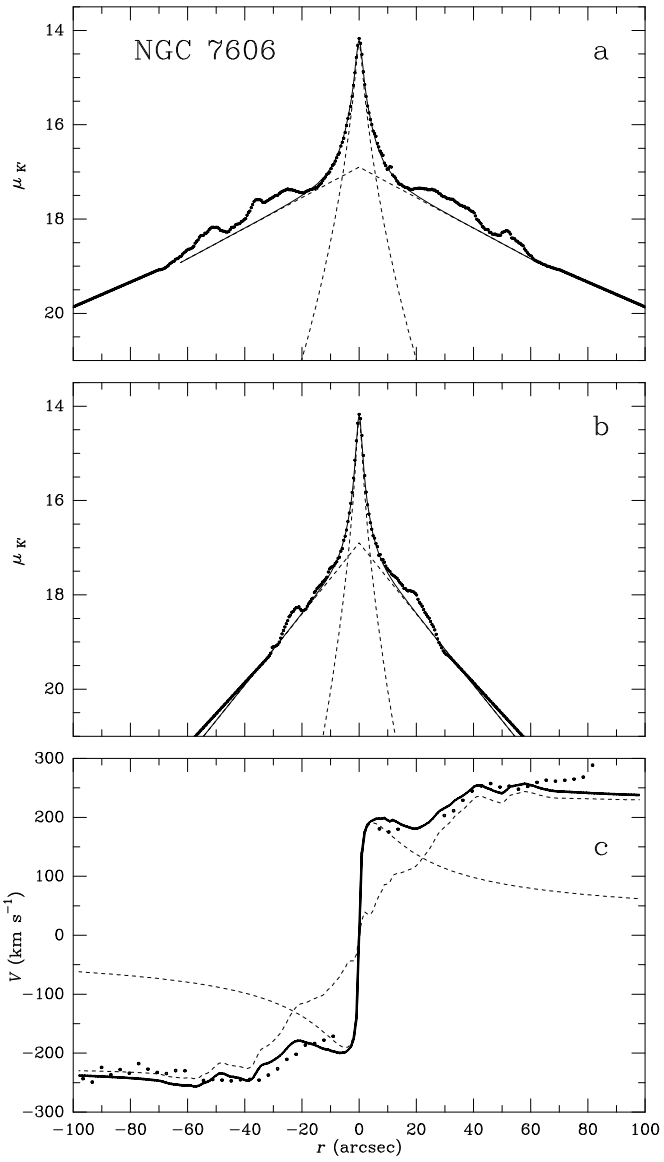

Fig. 6a–c. Same as Fig. 1, for NGC 7606

asymmetries and wiggles accounted for (the typical rms residual is $\lesssim 20$ km s^{-1}).

6.2. The mass-to-light ratios

Our data do not bring out a difference in the $\mathscr{M}/L$ ratios of the axisymmetric disk and the spiral arm components; this is partly due to the limited resolution, and partly to the oversimplified assumptions regarding the circularity of the rotation. Our analysis is thus limited to the determination of $(\mathscr{M}/L)_{\rm B}$ and $(\mathscr{M}/L)_{\rm D}$, the bulge and disk+arm mass-to-light ratios, respectively.

Our average disk $\mathscr{M}/L$ is 1.1 (from 'solution 3' for NGC 6788 and NGC 6810, and 'solution 2' for the four other galaxies): it is close to the value expected from analyses not relying on rotation (Appendix A, .2.), and close to recent direct determinations from NIR data and rotation (Gnedin et al. 1995; Quillen 1996); this average value is also consistent with the mean dark-matter content expected for these bright galaxies (Sect. 2.1). $(\mathscr{M}/L)_{\rm D}$ has a scatter of $\simeq 0.3$, a value only slightly larger than the a priori uncertainty attached to the distance determinations on these galaxies. Although our sample is, by far, too reduced for a statistical extrapolation, this is consistent with previous works finding evidence for a narrow range of disk $\mathscr{M}/L$ ratios (e.g., Chiba & Yoshi 1995; Broiels & Courteau 1997).

The determination of the bulge $\mathscr{M}/L$ ratio is sometimes troublesome. For the four galaxies with relatively small bulges, the solution of assigning the same ratio to the bulge and to the disk is not incompatible with the kinematical data; the bulge mass, anyway, is not critical as far as the whole galaxy mass is concerned: 'solution 1' and 'solution 2' produce $(\mathscr{M}/L)_{\rm D}$

values within $\simeq$ 10 % of each other. This shows that small adjustments to the assumed bulge $\mathscr{M}/L$ ratio, when needed for the fit (e.g. Broiels & Courteau 1997), are unable to significantly bias the derived total masses. But for the two galaxies with a bulge representing almost half the total luminosity, the problem is more critical: for NGC 6788, 'solution 2' is questionable, and for NGC 6810, it is unsatisfactory. The luminosity correction considered in Sect. 4.3 provides a qualitative solution; it can also be used to mimic a gradual decrease of the $\mathscr{M}/L$ ratio toward the center, e.g., as the result of an increasing metallicity (Table 4). This possibility has already been considered (Giovanardi & Hunt 1996), but bulges have been shown to be very similar to the disks in terms of colors (Peletier & Balcells 1996), at least at $r \approx r_{\rm e}$, and one may be wondering if this could be drastically different at the very center.

6.3. The kinematical data

Two-dimensional data on the gas kinematics would provide much tighter constraints on the $\mathscr{M}/L$ ratio of bulges and disks (and maybe even arms?) than do the major-axis spectra used in the present work. Such data (which are, unfortunately, available for only a very limited sample of objects) would also deserve, and require, proper attention to the radial streaming motions in the vicinity of spiral arms.

Due to the scarcity of observations, stellar spectroscopy of the bulge puts loose constraints on the mass of this component; the lack of available mean rotation, in particular, prevents an accurate determination of its dynamical status. The observations, anyway, are only one aspect of the question: establishing a relevant model including the disk potential may not be straightforward. Our simplified modelling has provided, in two cases out of three, a rather low $(\mathscr{M}/L)_{\rm B}$, as found from the unconstrained fit to the gas kinematics.

7. Conclusion

We have analyzed six bright spiral galaxies for which NIR and I-band surface photometry is available, together with a detailed gas rotation curve; these data provide the opportunity to study the overall distribution of stellar masses, with a priori little of the biasing effects due to extinction (in the central regions), and to dark matter (in the outer regions). Our results are summarized as follows.

We have carefully mapped the luminosity, with axisymmetric and non-axisymmetric components. The mass-to-light ratio of the disk within its optical extent is found close to what is expected for an old stellar population; the technique can thus be extended to the detailed study of lower-luminosity objects for which the dark-matter content is expected to be much higher.

In our small-bulge galaxies, there is marginal evidence for the mass-to-light ratio of the bulge being $\approx$ 20% lower than that of the disk. However, better kinematical data (stellar spectroscopy and 2D gas motions) are needed to confirm this. In early-type spirals with a large bulge, there is a stronger discrepancy with the gas rotation, even at $r \approx r_{\rm e}$(bulge), and deep stellar spectroscopy seems required to provide velocity dispersion constraining the mass, and metallicity gradients constraining the $\mathscr{M}/L$ ratio.

Acknowledgements. We are indebted to D.S. Mathewson and V.L. Ford for providing us with an electronic version of the MFB92 data. We thank the referee, M. Persic, for his valuable comments on the first version of the manuscript; we thank Ph. Prugniel for useful discussions. We have made use of the Lyon-Meudon Extragalactic Database supplied by the *LEDA* team at the Observatoire de Lyon.

Appendix A: NIR $\mathscr{M}/L$ ratios

We list a few determinations of K-band $\mathscr{M}/L$ ratios, both observational and theoretical. When relevant, the quoted $\mathscr{M}/L_K$ values (in solar units) have been converted from another passband and/or corrected to the system of absolute luminosities given by Worthey (1994): $M_\odot$=5.51, 4.84, 4.48, 3.37, and 3.33, in B, V, R, H, and K, respectively; they have also been corrected to H_0 = 75 km s^{-1} Mpc^{-1}.

A.1. Early-type galaxies and bulges

Quite different values have been published, and we present a selection which, although far from complete, is likely to be representative: Table 4 collects $\mathscr{M}/L_K$ determinations from various methods. A few works have calculated ratios involving a column luminosity (along the line of sight) and a spherical or spheroidal mass (from, e.g., the virial relation or a rotation velocity). We have thus corrected the luminosity to the same volume as the mass determination, in order to get physical $\mathscr{M}/L$ values. For the isothermal sphere, the correction is independent of the radius of the column and is equal to $2/\pi$; for the $r^{1/4}$ law, it depends on r: $\simeq 0.6$ at $r/r_{\rm e} = 0.1$, $\simeq 0.8$ at $r/r_{\rm e} = 1$. It is unlikely that any of these two luminosity laws fits the galaxies accurately; nevertheless, mean values from the above, applied globally to the samples, provide a crude but convenient first-order correction. For the isothermal sphere, we have thus multiplied the published ratios by 1.6, and for the $r^{1/4}$ law by 1.4. We note, however, that this crude correction is not free of bias, and the lower $\mathscr{M}/L$ value found in Table 4 for early-type bulges with respect to late-type ones could be due to geometrical effects on the line of sight, playing a different role in the case of a prominent bulge; we thus consider this evidence of a lower $\mathscr{M}/L$ as marginal.

A.2. Spiral-galaxy disks

We mention two studies not relying on rotation-curve fits.

– The Galactic disk in the solar vicinity: Kuijken & Gilmore (1989). From an analysis of star counts and stellar motions, these authors derive a column density (perpendicularly to the disk) of 35 $\mathscr{M}_\odot$pc^{-2} for the stars, and 48 $\mathscr{M}_\odot$pc^{-2} for all the accountable mass (mostly stars and gas). With the V column luminosities used by Bahcall (1984), and with $V-K$ = 2.0 (Thronson & Greenhouse 1988), $\mathscr{M}/L_K \simeq$

Table 4. A selection of NIR $\mathscr{M}/L$ ratios for ellipticals and bulges

Reference	Object(s)	Number	$\mathscr{M}/L_K$	Range / comments	Method
Devereux et al. (1987)	Es-S0s	35	1.20 [(a,c)]	nucleus ($r < 200$ pc)	velocity dispersion
,,	Sa-Sb bulges	6	0.70 [(a,d)]	,,	,,
,,	Sb-Sc bulges	10	0.90 [(a,d)]	,,	,,
Giovanardi & Hunt (1996)	Sa-Sab bulges [(e)]	7	0.70 [(b,d)]	$r \lessapprox \frac{1}{2}\, r_{\rm e}$ to $\frac{3}{2}\, r_{\rm e}$	gas rotation
Giovanardi & Hunt (1988)	Sc bulges	9	1.00 [(b,d)]	,,	,,
Oliva et al. (1995)	Es	4	1.04 [(a,c)]	nucleus	velocity dispersion
,,	normal bulges	3	0.84 [(a,d)]	,,	,,
,,	Seyfert-2 bulges	6	0.42 [(a,d)]	,,	,,
van der Marel(1991)	Es/S0s	37	1.20 [(f)]	$r \lessapprox r_{\rm e}$	dynamical model
Kormendy (1988) + Emsellem et al. (1996)	M104 (Sa)	–	0.83 [(g)]	$0.7 < r < 8''$	dynamical model
Kormendy & Richtone (1992) + Capaccioli et al. (1993)	NGC 3115 (S0)	–	1.20 [(h)]		dynamical model
Worthey (1994)	model elliptical	–	1.06	12 Gyr, [Fe/H] = 0.00	single-burst model
,,	,,	–	0.87	12 Gyr, [Fe/H] = 0.25	,,

Notes. Listed values follow the conventions of Appendix A. [(a)] after global luminosity correction corresponding to the isothermal sphere (Appendix A.1). [(b)] after global luminosity correction corresponding to the $r^{1/4}$ law (Appendix A.1). [(c)] from $\mathscr{M}/L_H$, with $H - K$ = 0.2. [(d)] from $\mathscr{M}/L_H$, with $H - K$ = 0.25. [(e)] including a Seyfert 1 (NGC 6814). [(f)] from a mean $\mathscr{M}/L_R$ = 2.97, with $R - K$ = 2.74 (average color calculated from de Vaucouleurs & Longo 1988 for 10 galaxies of this sample, and from Peletier et al. 1990 for another sample). [(g)] $\mathscr{M}/L_V \simeq 5.0$ at a few arcsec outside the nucleus (even if this region is dominated by a nuclear disk, it should be representative of the bulge population); with $V - K$ = 3.45 (Hes & Peletier 1993). [(h)] from $\mathscr{M}/L_B \simeq 6$, with $B - K$ = 4.21 (Bothun & Gregg 1990); adopted distance: 7.6 Mpc.

1.0 and 1.3 for the stars and for all accountable mass, respectively.

– Model disk: Jablonka & Arimoto (1992). For a pure Sb disk population, these authors derive from their evolutionary model a value of $\mathscr{M}/L_B \simeq 5.2$; with an average $B - K$ = 3.96 (Peletier & Balcells 1996), $\mathscr{M}/L_K \simeq 1.0$.

From the above, the expected value of $\mathscr{M}/L_K$ is $\simeq 1$ for both bulge and disk, in non-AGN galaxies.

Appendix B: mass and luminosity of Seyfert bulges

For a sample of Seyfert bulges, Nelson & Whittle (1996) found an offset of $\simeq 0.7$ mag in the σ vs. L relation (central velocity dispersion vs. bulge luminosity: the Faber-Jackson relation) with respect to non-Seyfert galaxies, and they interpret it as a lower $\mathscr{M}/L$ in galaxies otherwise 'normal' in terms of bulge-to-disk luminosity ratios. An alternative interpretation is that the stellar population of the bulge is the same as in other galaxies, but that the central luminosity is enhanced by the presence of the AGN. Indeed, the flux from the nucleus and its vicinity can be significantly increased, especially in the K band, by a) the presence of red supergiants from extranuclear starbusts (e.g., Hunt & Giovanardi 1992; Oliva et al. 1995), or b) a non-stellar contribution, like reradiation of shorter-wavelength light by hot dust (e.g., Hunt & Giovanardi 1992; Kotilainen at al. 1992; Kotilainen & Prieto, 1995).

References

Afanasiev, V.L., Sil'chenko, O.K., Zasov, A.V. 1989, A&A 213, L9
Andredakis, Y.C., Peletier, R., Balcells, M. 1995, MNRAS 275, 874
Bahcall, J.N. 1984, ApJ 276, 169
Bertola, F., Cinzano, P., Corsini, E.M. 1995, ApJ 448, L13
Binney, J., Tremaine, S. 1987, Galactic dynamics, Princeton Univ. Press, Princeton
Bothun, G.D., Gregg, M.D. 1990, ApJ 350, 73
Brandt, J.C. 1960, ApJ 131, 293
Broiels, A.H., Courteau, S. 1997, in Salucci, P. & Persic, M. (Eds.) The distribution of dark and visible mass in galaxies, ASPCS, in press
Buchhorn, M., Mathewson, D.S. 1992, unpublished, cited by Freeman (1992)
Burbidge, E.M., Burbidge, G.R., Prendergast, K.H. 1959, ApJ 130, 739
Capaccioli, M., Cappellaro, E., Held, E.V., Vietri, M. 1993, A&A 274, 69
Chiba, M., Yoshi, Y. 1995, ApJ 442, 82
de Jong, R.S. 1996, A&AS 118, 557
de Vaucouleurs, A., Longo, G. 1988, Catalogue of visual and infrared photometry of galaxies from 0.5 μm to 10 μm (1961-1985), The University of Texas Monographs in Astronomy, No. 5
Devereux, N., Becklin, E.E., Scoville, N. 1987, ApJ 312, 529
Emsellem, E., Bacon, R., Monnet, G., et al. 1996, A&A 312, 777
Fillmore, J.A., Boroson, T.A., Dressler, A. 1986, ApJ 302, 208
Freeman, K.C. 1970, ApJ 160, 811
Freeman, K.C. 1992, in Thuan, T.X., Balkowski, Ch., Tran Than Van, J. (Eds.), Physics of nearby galaxies: Nature or nurture? (Frontières, Gif-sur-Yvette), p. 201
Giovanardi, C., Hunt, L.K. 1988, AJ 95, 408
Giovanardi, C., Hunt, L.K. 1996, AJ 111, 1086 (GH)
Gnedin, O.Y., Goodman, J., Frei, Z. 1995, AJ 110, 1105
Héraudeau, Ph., Simien, F. 1995, Astro. Lett. & Communications 31, 219
Héraudeau, Ph., Simien, F. 1996, A&AS 118, 111
Héraudeau, Ph., Simien, F., Mamon, G.A. 1996a, A&AS 117, 417 (HSMa)

Héraudeau, Ph., Simien, F., Mamon, G.A. 1996b, in Minniti, D., Rix, H.-W. (Eds.) Spiral galaxies in the near infrared, Springer, Berlin, p. 235 (HSMb)
Héraudeau, Ph., Simien, F., Mamon, G.A. 1996c, in Minniti, D., Rix, H.-W. (Eds.) Spiral galaxies in the near infrared, Springer, Berlin, p. 248
Hes, R., Peletier, R.F. 1993, A&A 268, 539
Hunt, L.K., Giovanardi 1992, AJ 104, 1018
Jablonka, P., Arimoto, N. 1992, A&A 255, 63
Kalnajs, A. 1983, in Athanassoula, E.A. (Ed.), Internal kinematics and dynamics of galaxies, Reidel, Dordrecht, p. 87
Kent, S.M. 1986, AJ 91, 1301
Kent, S.M. 1987, AJ 93, 816
Kent, S.M. 1988, AJ 96, 514
Kormendy, J. 1988, ApJ 335, 40
Kormendy, J., Bender, R., Ajhar, E.A., et al. 1996, ApJ 473, L91
Kormendy, J., Richstone, D. 1992, ApJ 393, 559
Kotilainen, J.K., Ward, M.J., Boisson, C., et al. 1992, MNRAS 256, 125
Kotilainen, J.K., Prieto, M.A. 1995, A&A 295, 646
Kormendy, J. 1988, ApJ 335, 40
Kuijken, K., Gilmore, G. 1989, MNRAS 239, 605
Lequeux, J. 1983, A&A 125, 394
Mathewson, D.S., Ford, V.L., Buchhorn, M. 1992, ApJS 81, 413 (MFB92)
McElroy, D. 1995, ApJS 100, 105
Monnet, G., Simien, F. 1977, A&A 56, 173
Nelson, C.H., Whittle, M. 1996, ApJ 465, 96
Oliva, E., Origlia, L., Kotilainen, J.K., Moorwood, A.F.M. 1955, A&A 301, 55
Peletier, R.F., Balcells, M. 1996, AJ 111, 2238
Peletier, R.F., Valentijn, E.A., Jameson, R.F. 1990, A&A 233, 62
Persic, M., Salucci, P. 1988, MNRAS 234, 131
Persic, M., Salucci, P. 1995, ApJS 99, 501
Persic, M., Salucci, P., Stel, F. 1996, MNRAS 281, 27 (PSS96)
Quillen, A.C. 1996, in Minniti, D., Rix, H.-W. (Eds.) Spiral galaxies in the near infrared, Springer, Berlin, p. 157
Rhoads, E.R. 1996, in Minniti, D., Rix, H.-W. (Eds.) Spiral galaxies in the near infrared, Springer, Berlin, p. 58
Rix, H.-W., Rieke, M.J. 1993, ApJ 418, 123
Rix, H.-W., Zaritsky, D. 1995, ApJ 447, 82
Rubin, V.C., Ford, W.K., Jr., Thonnard, N 1980, ApJ 238, 471
Rubin, V.C., Graham, J.A. 1987, ApJ 316, L67
Schmidt, M.1956, Bull. Astron. Inst. Neth. 13, 15
Sérsic, J.-L. 1968, Atlas de galaxias australes, Observatorio Astronómico de Córdoba
Simien, F., Héraudeau, Ph. 1994, La Lettre de l'OHP No. 13, p.1
Sofue, Y. 1996, ApJ 458, 120
Thronson, H.A. Jr., Greenhouse, M.A. 1988, ApJ 327, 671
van der Marel, R.P. 1991, MNRAS 253, 710
van der Kruit, P.C., Searle, L. 1981, A&A 95, 105
Wielen, R. 1976, in Kharadze, E.D. (Ed.), Stars and galaxies from observational points of view, p. 402
Whitmore, B.C., Malumuth, E. 1984, unpublished (quoted in McElroy 1995)
Whitmore, B.C., Rubin, V.C. 1985, unpublished (quoted in McElroy 1995)
Worthey, G. 1994, ApJS 95, 107

This article was processed by the author using Springer-Verlag LaTeX A&A style file *L-AA* version 3.